

Fibroblast-Activation Protein PET and Histopathology in a Single-Center Database of 324 Patients and 21 Tumor Entities

Nader Hirmas¹, Rainer Hamacher², Miriam Sraieb¹, Marc Ingenwerth³, Lukas Kessler¹, Kim M. Pabst¹, Francesco Barbatto¹, Katharina Lueckerath¹, Stefan Kasper², Michael Nader¹, Hans-Ulrich Schildhaus^{3,4}, Claudia Kesck⁵, Bastian von Tresckow⁶, Christine Hanoun⁶, Hubertus Hautzel¹, Clemens Aigner⁷, Martin Glas⁸, Martin Stuschke⁹, Sherko Kümmel¹⁰, Philipp Harter¹¹, Celine Lugnier¹², Waldemar Uhl¹³, Marco Niedergethmann¹⁴, Boris Hadaschik⁵, Viktor Grünwald⁵, Jens T. Siveke^{15,16}, Ken Herrmann¹, and Wolfgang P. Fendler¹

¹Department of Nuclear Medicine, University of Duisburg–Essen, and German Cancer Consortium (DKTK)–University Hospital Essen, Essen, Germany; ²Department of Medical Oncology, West German Cancer Center, University of Duisburg–Essen, and DKTK–University Hospital Essen, Essen, Germany; ³Institute of Pathology, University Hospital Essen, Essen, Germany; ⁴Targos Molecular Pathology Inc., Kassel, Germany; ⁵Department of Urology, University of Duisburg–Essen, and DKTK–University Hospital Essen, Essen, Germany; ⁶Department of Hematology and Stem Cell Transplantation, University of Duisburg–Essen, and DKTK–University Hospital Essen, Essen, Germany; ⁷Department of Thoracic Surgery and Thoracic Endoscopy, University of Duisburg–Essen, and DKTK–University Hospital Essen, Essen, Germany; ⁸Division of Clinical Neurooncology, Department of Neurology, University of Duisburg–Essen, and DKTK–University Hospital Essen, Essen, Germany; ⁹Department of Radiation Therapy, University of Duisburg–Essen, and DKTK–University Hospital Essen, Essen, Germany; ¹⁰Breast Unit, Kliniken Essen–Mitte, Essen, Germany, and Department of Gynecology with Breast Center, Charité–Universitätsmedizin Berlin, Berlin, Germany; ¹¹Department of Gynecology and Gynecologic Oncology, Evang. Kliniken Essen–Mitte, Essen, Germany; ¹²Department of Hematology and Oncology with Palliative Care, Ruhr University Bochum, Bochum, Germany; ¹³Department of General and Visceral Surgery, Ruhr University Bochum, Bochum, Germany; ¹⁴Clinic for General and Visceral Surgery, Alfried Krupp Hospital, Essen, Germany; ¹⁵Bridge Institute of Experimental Tumor Therapy, West German Cancer Center, University Hospital Essen, Essen, Germany; and ¹⁶Division of Solid Tumor Translational Oncology, DKTK (Partner Site Essen) and German Cancer Research Center, Heidelberg, Germany

We present an overview of our prospective fibroblast-activation protein inhibitor (FAPi) registry study across a 3-y period, with head-to-head comparison of tumor uptake in ⁶⁸Ga-FAPi and ¹⁸F-FDG PET, as well as FAP immunohistochemistry. **Methods:** This is an interim analysis of the ongoing ⁶⁸Ga-FAPi PET prospective observational trial at our department. Patients who underwent clinical imaging with ⁶⁸Ga-FAPi PET between October 2018 and October 2021 were included. Tracer uptake was quantified by SUV_{max} for tumor lesions and by SUV_{mean} for normal organs. PET tumor volume (40% isocontour) and tumor-to-background ratios were calculated. Correlation between SUV_{max} and FAP staining in tissue samples was analyzed. **Results:** In total, 324 patients with 21 different tumor entities underwent ⁶⁸Ga-FAPi imaging; 237 patients additionally received ¹⁸F-FDG PET. The most common tumor entities were sarcoma (131/324, 40%), pancreatic cancer (67/324, 21%), and primary tumors of the brain (22/324, 7%). The mean primary tumor SUV_{max} was significantly higher for ⁶⁸Ga-FAPi than ¹⁸F-FDG among pancreatic cancer (13.2 vs. 6.1, $P < 0.001$) and sarcoma (14.3 vs. 9.4, $P < 0.001$), and the same was true for mean SUV_{max} in metastatic lesions of pancreatic cancer (9.4 vs. 5.5, $P < 0.001$). Mean primary tumor maximum tumor-to-background ratio was significantly higher for ⁶⁸Ga-FAPi than ¹⁸F-FDG across several tumor entities, most prominently pancreatic cancer (14.7 vs. 3.0, $P < 0.001$) and sarcoma (17.3 vs. 4.7, $P < 0.001$). Compared with ¹⁸F-FDG, ⁶⁸Ga-FAPi showed superior detection for locoregional disease in sarcoma (52 vs. 48 total regions detected) and for distant metastatic disease in both sarcoma (137 vs. 131) and pancreatic cancer

(65 vs. 57), respectively. Among 61 histopathology samples, there was a positive correlation between ⁶⁸Ga-FAPi SUV_{max} and overall FAP immunohistochemistry score ($r = 0.352$, $P = 0.005$). **Conclusion:** ⁶⁸Ga-FAPi demonstrates higher absolute uptake in pancreatic cancer and sarcoma, as well as higher tumor-to-background uptake along with improved tumor detection for pancreatic cancer, sarcoma, and other tumor entities when compared with ¹⁸F-FDG. ⁶⁸Ga-FAPi is a new tool for tumor staging with theranostic potential.

Key Words: FAPi; PET; oncology; staging; theranostic

J Nucl Med 2023; 64:711–716

DOI: 10.2967/jnumed.122.264689

Imaging is critically important in the diagnosis and staging of malignancies, with varying detection rates depending on the tumor entity and diagnostic modality. PET of cancer cells using ¹⁸F-FDG PET acquires additional molecular information useful for the management of disease and for improving treatment outcomes (1–3).

Tumor growth and spread are determined not only by cancer cells but also by the tumor microenvironment, which contains several nonmalignant components. Besides immune cells, important constituents are cancer-associated fibroblasts, which are known to be involved in tumor growth, migration, and progression (4). Although heterogeneous in their origin, cancer-associated fibroblasts have common properties that are distinct from normal fibroblasts, expressing proteins not found in their normal counterparts (5). A subpopulation of cancer-associated fibroblasts expresses, among other markers, fibroblast-activation protein (FAP) α (FAP α), which is associated with protumorigenic functions (6–10).

Received Jul. 18, 2022; revision accepted Nov. 8, 2022.

For correspondence or reprints, contact Wolfgang P. Fendler (wolfgang.fendler@uk-essen.de).

Published online Dec. 29, 2022.

COPYRIGHT © 2023 by the Society of Nuclear Medicine and Molecular Imaging.

Therefore, these cells represent attractive diagnostic and therapeutic targets. Since 2018, preclinical and clinical data have emerged on a variety of FAP-directed therapies, including radiolabeled, low-molecular-weight FAP inhibitors (FAPIs), further underlining their favorable properties in diagnosis and therapy (11–15).

Data for the superiority of ⁶⁸Ga-FAPI PET over conventional imaging have been reported previously in small cohorts (13,16). On the basis of the favorable imaging characteristics of ⁶⁸Ga-FAPI PET, patients were referred for clinical ⁶⁸Ga-FAPI PET staging both at initial diagnosis and after intervention and were offered enrollment in our prospective observational ⁶⁸Ga-FAPI registry. Clinical indications for ⁶⁸Ga-FAPI PET were staging of disease in high-risk patients, evaluation of the localization of tumor lesions before biopsy or surgery, further workup of equivocal imaging results, or evaluation of therapeutic options.

In this report, we present the largest cohort to date (to our knowledge), with an overview of the tumor entities diagnosed and staged with ⁶⁸Ga-FAPI across a 3-y period, including head-to-head comparison of tumor uptake in ⁶⁸Ga-FAPI and ¹⁸F-FDG PET, as well as FAP immunohistochemistry.

MATERIALS AND METHODS

Study Design and Participants

Patients underwent imaging with ⁶⁸Ga-FAPI PET between October 2018 and October 2021 at the Department of Nuclear Medicine at the University Hospital Essen. This is an interim analysis of the ongoing ⁶⁸Ga-FAPI PET observational trial conducted at the University Hospital Essen (NCT04571086). Until October 2021, adult patients who underwent clinical ⁶⁸Ga-FAPI PET were offered the possibility to consent to a prospective observational trial for correlation and clinical follow-up of PET findings. Evaluation of data was approved by the ethics committee of the University Duisburg–Essen (approvals 20-9485-BO and 19-8991-BO). Patient subgroups have been reported in previous publications ($n = 47$ (17), $n = 69$ (18), and $n = 91$ (19)).

Details of data collection (20–22); imaging and administration of radioligands (18,23,24); imaging analysis, immunohistochemistry, and FAP scoring (17,25); and statistical analysis (26) are provided in the supplemental materials (available at <http://jnm.snmjournals.org>).

RESULTS

Patient Characteristics

Three hundred twenty-four patients were included; their characteristics are outlined in Table 1. The median age was 59 y (interquartile range, 16 y). The most common tumor entity was sarcoma (131/324, 40%), followed by primary tumors of the pancreas (67/324, 21%), brain (22/324, 7%), and lung (14/324, 4%) and pleural mesothelioma (12/324, 4%). Most patients (235/324, 73%) underwent ⁶⁸Ga-FAPI PET imaging for restaging purposes. A breakdown of histopathologic diagnoses, as well as the presence of primary and metastatic lesions for each category, is provided in Supplemental Table 1.

Tumor Diagnostics and ⁶⁸Ga-FAPI PET

The mean SUV_{max} for primary lesions and metastatic lesions on ⁶⁸Ga-FAPI PET is shown in Figures 1A and 1B, respectively. Mean values of primary tumor SUV_{max} ranged from 3.41 for brain tumors to 21.44 for ovarian tumors. The mean primary tumor SUV_{max} was higher than 10 for 9 of 17 (53%) tumor entities with primary lesions, including prostate (10.4), bladder (10.5), pancreas (13.2), and sarcoma (14.1), among others. The mean SUV_{max} for primary lesions and metastatic lesions using broader subgroups is provided in Supplemental Figure 1.

TABLE 1
Patient Characteristics ($n = 324$)

Variable	Data
Sex	
Male	168 (52%)
Female	156 (48%)
Median age at ⁶⁸ Ga-FAPI scan (y)	59 (16)
Tumor entity	
Sarcoma	131 (40%)
Pancreas	67 (21%)
Brain	22 (7%)
Lung	14 (4%)
Pleura	12 (4%)
Cholangiocellular	11 (3%)
Colorectal	11 (3%)
Prostate	11 (3%)
Head and neck	9 (3%)
Bladder	8 (3%)
Lymphoma	7 (2%)
Myeloma	6 (2%)
Ovarian	4 (1%)
Breast	3 (1%)
Duodenum	2 (1%)
Other*	6 (2%)
Tumor staging with ⁶⁸Ga-FAPI scan[†]	
No evidence of disease	19 (8%)
Stage I	26 (10%)
Stage II	29 (12%)
Stage III	25 (10%)
Stage IV	149 (60%)
Scanning purposes	
Staging at initial diagnosis	88 (27%)
Restaging after therapy	235 (73%)
Prior therapy received	
None	88 (27%)
Surgery	176 (55%)
Chemotherapy	176 (55%)
Radiation therapy	83 (26%)
Immune therapy	27 (8%)
Hormone therapy	9 (3%)
Radionuclide therapy	3 (1%)
Median uptake time (min)	
⁶⁸ Ga-FAPI	14 (24)
¹⁸ F-FDG	67 (23)
Median time between ⁶⁸ Ga-FAPI and ¹⁸ F-FDG (d)	0 (2)

*Tumors of cervix ($n = 1$), liver ($n = 1$), skin ($n = 1$), thyroid ($n = 1$), and stomach ($n = 1$) and myoepithelial carcinoma of knee ($n = 1$).

[†]Among 7 most common tumor entities ($n = 248$), excluding brain tumors as well as 9 sarcoma patients (not stageable according to AJCC-8).

Qualitative data are number and percentage; continuous data are median and interquartile range.

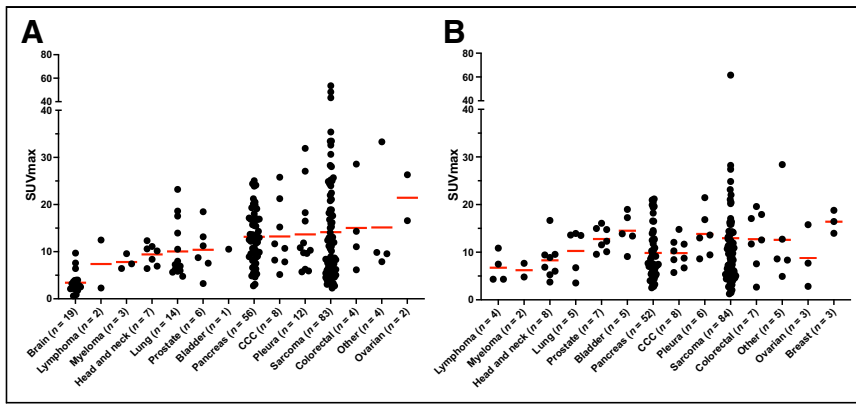


FIGURE 1. Mean SUV_{max} on ^{68}Ga -FAPI PET for primary lesions ($n = 221$) (A) and hottest metastatic lesions per patient ($n = 199$) (B). Data points represent hottest lesions for individual patients. Data in A and B were sorted by mean SUV_{max} in A. Numbers of patients included for every tumor entity are given on x-axis. Red lines represent mean values. y-axis is split to account for extreme values. Primary and metastatic lesions for every tumor entity are provided in Supplemental Table 1.

Staging by ^{68}Ga -FAPI PET is presented in Supplemental Figure 2 for the 7 most common tumor entities in our registry (with at least 10 patients, excluding brain tumors). In our prospective cohort, distant metastatic disease was detected in most patients with head and neck cancer (8/9, 89%), pancreatic cancer (44/67, 66%), sarcoma (79/122, 65%), colon or rectal cancer (7/11, 64%), prostate cancer (7/11, 64%), bladder cancer (5/8, 63%), and cholangiocellular carcinoma (CCC, 6/11, 55%). Locoregional-only disease was detected most often in lung carcinoma (11/14, 79%) and in pleural mesothelioma (9/12, 75%).

^{68}Ga -FAPI PET Versus ^{18}F -FDG PET Imaging

In our cohort, 237 of 324 patients (73%) had undergone additional ^{18}F -FDG PET, and a head-to-head analysis of both imaging modalities was performed. Mean SUV_{max} was significantly higher for ^{68}Ga -FAPI than for ^{18}F -FDG PET among primary tumors of the pancreas (13.2 vs. 6.1, $P < 0.001$) and sarcoma (14.3 vs. 9.4, $P < 0.001$), as shown in Figure 2A. Similarly, the mean SUV_{max} in metastatic lesions was significantly higher for ^{68}Ga -FAPI than for ^{18}F -FDG in pancreatic cancer (9.4 vs. 5.5, $P < 0.001$; Fig. 2B).

For primary tumors, mean tumor-to-background ratio (TBR_{max}) (with blood pool background) was significantly higher for ^{68}Ga -FAPI than for ^{18}F -FDG in pancreatic cancer (9.9 vs. 3.5, $P < 0.001$) and

as shown in Figure 4A. Mean TBR_{max} (with liver background) was also significantly higher for ^{68}Ga -FAPI than for ^{18}F -FDG in pancreatic cancer (10.6 vs. 2.8, $P < 0.001$) and sarcoma (18.9 vs. 4.7, $P = 0.003$), in addition to prostate cancer (15.1 vs. 4.9, $P < 0.001$), pleural mesothelioma (13.5 vs. 4.8, $P = 0.017$), and CCC (14.5 vs. 3.9, $P = 0.012$), as shown in Figure 4B. Conversely, mean TBR_{max} (with muscle background) was significantly lower for ^{68}Ga -FAPI than for ^{18}F -FDG in pleural mesothelioma (9.4 vs. 17.8, $P = 0.027$), prostate cancer (8.0 vs. 15.6, $P = 0.009$), and CCC (10.0 vs. 15.4, $P = 0.024$), as shown in Figure 4C.

There were no significant differences between metabolic tumor volumes measured for primary lesions and metastatic lesions in ^{68}Ga -FAPI and ^{18}F -FDG PET scans across tumor entities, as shown in Supplemental Figure 3.

Examples of ^{68}Ga -FAPI and ^{18}F -FDG PET scans showing tumor uptake and FAP α staining in tumor samples are presented in Supplemental Figures 4–8.

A comparison of primary SUV_{max} and involved regions between ^{68}Ga -FAPI and ^{18}F -FDG PET among metastatic and nonmetastatic disease and across tumor entities is provided in Supplemental Table 2. When compared with ^{18}F -FDG, ^{68}Ga -FAPI showed superior detection for locoregional disease in sarcoma (52 vs. 48 total regions detected) and for distant metastatic disease in sarcoma (137 vs. 131), pancreatic cancer (65 vs. 57), head and neck cancer (15 vs. 13), CCC (12 vs. 11), lung cancer (9 vs. 8), and bladder cancer (8 vs. 7). However, ^{68}Ga -FAPI showed inferior detection of lymphoma compared with ^{18}F -FDG (7 vs. 10).

Immunohistochemistry and FAP Scoring

Sixty-one tissue samples dated within 3 mo from the date of ^{68}Ga -FAPI PET (median, 20.5 d; interquartile range, 23 d) were analyzed and scored (sarcoma, $n = 33$; pancreas, $n = 11$; pleura, $n = 5$; urothelium, $n = 4$; colon or rectum, $n = 3$; head and neck, $n = 3$; prostate, $n = 1$; and lung, $n = 1$). The corresponding SUV_{max} on ^{68}Ga -FAPI PET measured for the specific lesions biopsied before or after ^{68}Ga -FAPI PET, or surgically removed after ^{68}Ga -FAPI PET, were included

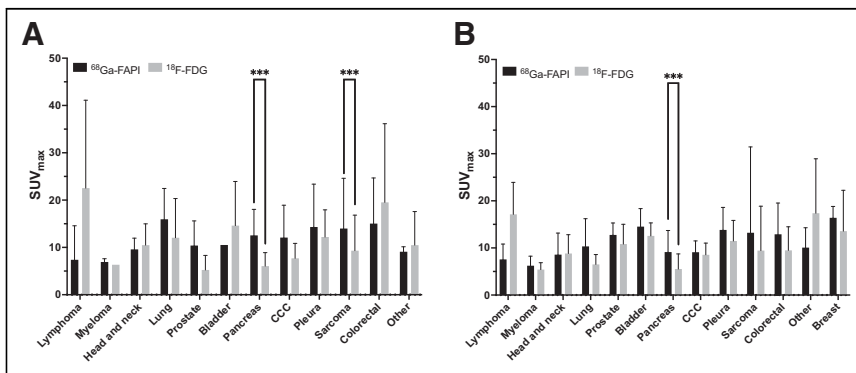


FIGURE 2. Comparison of mean SUV_{max} for primary lesions (A) and metastatic lesions (B) between ^{68}Ga -FAPI and ^{18}F -FDG PET across tumor entities. Entities are arranged as presented in Figure 1. Mean and SD are presented for every bar. Two-tailed paired t test was performed. * $P < 0.05$. ** $P < 0.01$. *** $P < 0.001$.

sarcoma (10.4 vs. 5.8, $P < 0.001$), as shown in Figure 3A. Mean TBR_{max} (with liver background) was also significantly higher for ^{68}Ga -FAPI than for ^{18}F -FDG in pancreatic cancer (14.7 vs. 3.0, $P < 0.001$) and sarcoma (17.3 vs. 4.7, $P < 0.001$), in addition to prostate cancer (7.8 vs. 2.7, $P = 0.017$), pleural mesothelioma (12.9 vs. 5.0, $P = 0.003$), head and neck cancer (14.5 vs. 4.2, $P = 0.013$), and CCC (19.5 vs. 3.6, $P = 0.016$), as shown in Figure 3B. Conversely, mean TBR_{max} (with muscle background) was significantly lower for ^{68}Ga -FAPI than for ^{18}F -FDG in pleural mesothelioma (9.4 vs. 17.6, $P = 0.004$; Fig. 3C).

For metastatic lesions, the mean TBR_{max} (with blood pool background) was significantly higher for ^{68}Ga -FAPI than for ^{18}F -FDG in pancreatic cancer (7.0 vs. 3.4, $P < 0.001$) and sarcoma (9.8 vs. 5.8, $P = 0.028$),

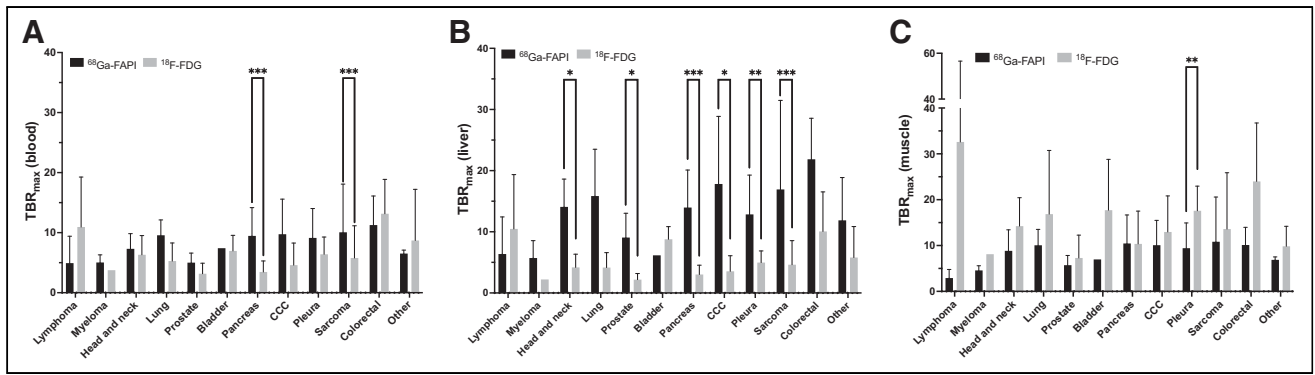


FIGURE 3. Comparison of mean TBR_{max} for primary lesions between ⁶⁸Ga-FAPI and ¹⁸F-FDG PET across tumor entities, with different reference backgrounds (blood [A], liver [B], and muscle [C]). Entities are arranged as presented in Figure 1. Mean and SD are presented for every bar. Two-tailed paired *t* test was performed. **P* < 0.05. ***P* < 0.01. ****P* < 0.001.

in the correlation analysis. Across the 61 samples, there was a significant positive correlation between the overall score for FAP α immunohistochemistry and ⁶⁸Ga-FAPI SUV_{max} ($r = 0.352$, $P = 0.005$, Fig. 5).

DISCUSSION

We report findings for 324 patients with 21 tumor entities diagnosed and staged by ⁶⁸Ga-FAPI PET as part of our registry study over a 3-y period, with a head-to-head analysis of ⁶⁸Ga-FAPI versus ¹⁸F-FDG PET uptake in tumor and metastatic lesions, as well as correlation between ⁶⁸Ga-FAPI uptake and FAP α expression in tissue samples. This represents the largest cohort, to our knowledge, of patients examined with this novel imaging modality. Our results demonstrate higher tumor-to-liver uptake ratios for ⁶⁸Ga-FAPI than for ¹⁸F-FDG in 6 of 14 (43%) of the evaluated tumor entities (most prominently sarcoma and pancreatic cancer, in addition to head and neck cancer, prostate cancer, CCC, and pleural mesothelioma) and comparable results in 8 of 14 (57%). Furthermore, we observed a positive correlation between radiotracer uptake and FAP α immunohistochemistry staining.

Relatively low ⁶⁸Ga-FAPI uptake in normal parenchyma improves tumor delineation, especially in regions with high physiologic glucose uptake. Thus, ⁶⁸Ga-FAPI demonstrates improved per-region tumor detection for pancreatic cancer, sarcoma, CCC, prostate

cancer, pleural mesothelioma, and head and neck cancer when compared with ¹⁸F-FDG. As such, ⁶⁸Ga-FAPI PET is a promising imaging modality for these entities, and it has the potential for more precise staging and management of patients, as well as therapeutic screening.

⁶⁸Ga-FAPI PET images the protein FAP α , which is located primarily on cancer-associated fibroblasts in the stroma, but this protein can also be found on tumor cells. High tumor uptake and low organ uptake support the potential use of FAPI ligands in a therapeutic context, particularly for sarcoma and pancreatic cancer. Use of FAP-directed radioligand therapy has been reported to be feasible for breast cancer (11), ovarian cancer (27), and sarcoma and pancreatic cancer (15,28), as well as multiple advanced and refractory tumors (14,29,30). All applications of FAP-directed radioligand therapy relied on baseline patient selection by high uptake on ⁶⁸Ga-FAPI PET. In addition, FAP-targeting drugs have been showing clinical promise across various tumor entities; 1 prominent example is talabostat, which has shown tumor control in 21% of patients with colorectal cancer (31). As such, future drug developments and their potential clinical applications may be enhanced through ⁶⁸Ga-FAPI imaging, which aids in selecting patients whose tumors exhibit high ⁶⁸Ga-FAPI uptake and low glycolytic phenotypes and who would potentially benefit from FAP-directed radioligand therapy.

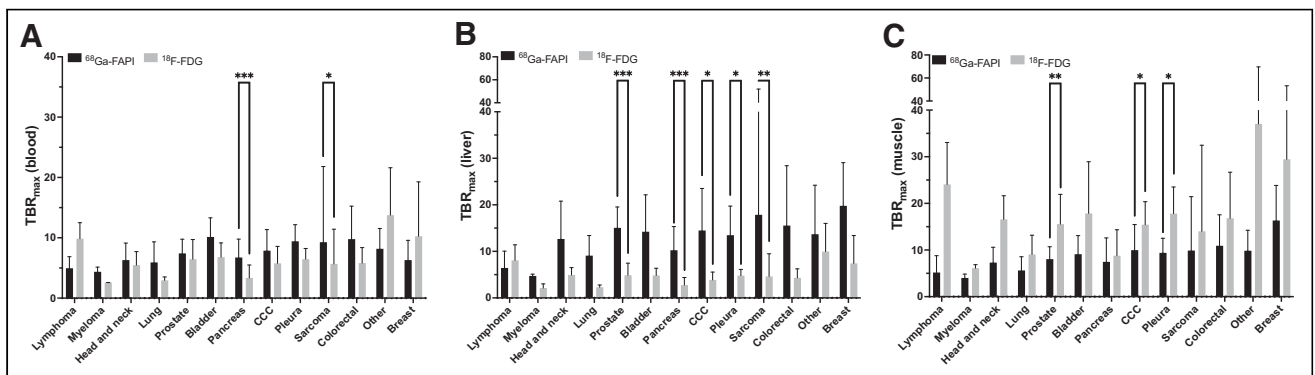


FIGURE 4. Comparison of mean TBR_{max} for metastatic lesions between ⁶⁸Ga-FAPI and ¹⁸F-FDG PET across tumor entities, with different reference backgrounds (blood [A], liver [B], and muscle [C]). Entities are arranged as presented in Figure 1. Mean and SD are presented for every bar. Two-tailed paired *t* test was performed. **P* < 0.05. ***P* < 0.01. ****P* < 0.001.

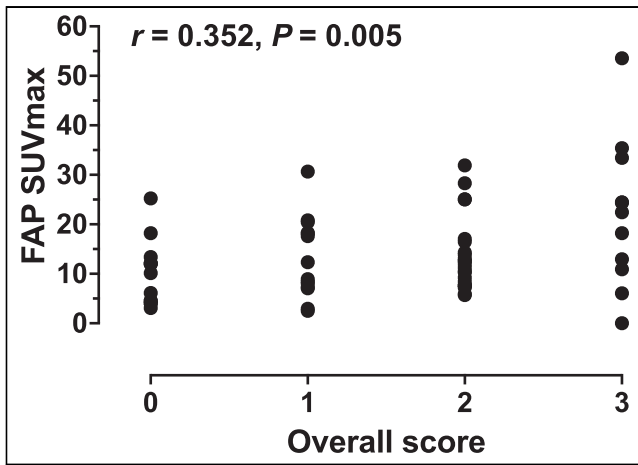


FIGURE 5. Correlation of ^{68}Ga -FAP- SUV_{max} with overall score for FAP-immunohistochemistry samples within 3 mo from ^{68}Ga -FAP- PET ($n = 61$). Overall FAP score refers to highest score assigned for tumor or stroma. r is Pearson correlation coefficient. Strength of correlation: negligible ($0.00 < r \leq \pm 0.29$), low ($\pm 0.30 \leq r \leq \pm 0.49$), moderate ($\pm 0.50 \leq r \leq \pm 0.69$), or high ($r \geq \pm 0.70$).

Another ongoing clinical trial at our department (NCT05160051) aims to explore the diagnostic accuracy of ^{68}Ga -FAP-46 PET and its impact on management and interreader reproducibility for different FAP-expressing tumor entities. Here, tumor samples will be collected within 8 wk from the time of the ^{68}Ga -FAP- PET scan to better elucidate the correlation between ^{68}Ga -FAP-46 uptake intensity and histopathologic FAP expression.

Our analysis has several limitations. SUV for ^{68}Ga -FAP-46 is reproducible at different time points (18) and is routinely measured but not yet a well-established metric. In addition, for some patient subgroups, there were low sample sizes and a referral bias. We report SUV s from different PET devices; despite cross calibration based on European Association of Nuclear Medicine Research Ltd. standards, SUV deviations may have occurred but were not statistically significantly (e.g., random samples with equal numbers of patients, $P = 0.949$). Moreover, the fact that quantitative immunohistochemistry assessment across all planes of whole-mount pathology specimens was not feasible may have led to deviations between ^{68}Ga -FAP- SUV_{max} and immunohistochemistry scores.

CONCLUSION

When compared with ^{18}F - FDG , ^{68}Ga -FAP-46 demonstrates higher absolute uptake in pancreatic cancer and sarcoma, as well as higher tumor-to-background uptake along with improved tumor detection for pancreatic cancer, sarcoma, CCC, prostate cancer, pleural mesothelioma, and head and neck cancer. A prospective clinical trial at our department (NCT05160051) is currently under way.

DISCLOSURE

Rainer Hamacher is supported by the Clinician Scientist Program of the University Medicine Essen Clinician Scientist Academy (UMEA) sponsored by the faculty of medicine and Deutsche Forschungsgemeinschaft (DFG) and has received travel grants from Lilly, Novartis, and Pharma Mar, as well as fees from Lilly

and Pharma Mar. Lukas Kessler is a consultant for AAA and BTG and received fees from Sanofi. Kim Pabst has received a Junior Clinician Scientist Stipend of UMEA sponsored by the Faculty of Medicine at the University of Duisburg–Essen and DFG, and he has received research funding from Bayer outside the submitted work. Katharina Lueckerath is a consultant for Sofie Biosciences and receives research funding from Curie Therapeutics. Stefan Kasper reports personal fees and grants from AstraZeneca, Merck Serone, Merck Sharpe & Dohme, Amgen, Bristol Myers Squibb, Roche, Lilly, Servier, Incyte, and SanofiAventis outside the submitted work. Claudia Kesck has received consultant fees from Apogepha, research funding from AAA/Novartis and Curie Therapeutics, and compensation for travel from Janssen R&D. Bastian von Tresckow is an advisor or consultant for Allogene, BMS/Celgene, Cerus, Incyte, Miltenyi, Novartis, Pentaxfarm, Roche, Amgen, Pfizer, Takeda, Merck Sharp & Dohme, and Gilead Kite; has received honoraria from AstraZeneca, Novartis, Roche Pharma AG, Takeda, and Merck Sharp & Dohme; reports research funding from Novartis, Merck Sharp & Dohme, and Takeda; and reports travel support from AbbVie, AstraZeneca, Kite-Gilead, Merck Sharp & Dohme, Takeda, and Novartis. Christine Hanoun received honoraria from BMS, Takeda, and AstraZeneca; travel grants from AbbVie; and research funding from Novartis. Hubertus Hautzel reports research funding and travel support from PARI GmbH outside the submitted work. Ken Herrmann reports personal fees from Bayer, SIRTEX, Adacap, Curium, Endocyte, IPSEN, Siemens Healthineers, GE Healthcare, Amgen, Novartis, ymabs, Aktis, Oncology, and Pharma15, as well as personal and other fees from Sofie Biosciences, nonfinancial support from ABX, and grants and personal fees from BTG, all of which are outside the submitted work. Boris Hadaschik has had advisory roles for ABX, AAA/Novartis, Astellas, AstraZeneca, Bayer, Bristol Myers Squibb, Janssen R&D, Lightpoint Medical, Inc., and Pfizer; has received research funding from Astellas, Bristol Myers Squibb, AAA/Novartis, the German Research Foundation, Janssen R&D, and Pfizer; and has received compensation for travel from Astellas, AstraZeneca, Bayer, and Janssen R&D. Philipp Harter reports grants, personal fees, and nonfinancial support from AstraZeneca and GSK; grants and personal fees from Roche, MSD, Clovis, and Immunogen; personal fees from Mersana, Sotio, Stryker, and Zai Lab; and grants from Boehringer Ingelheim, Medac, Genmab, Deutsche Krebshilfe, Deutsche Forschungsgemeinschaft, and the European Union, all of which are outside the submitted work. Jens T. Siveke received honoraria as a consultant or for continuing medical education presentations from AstraZeneca, Bayer, Bristol-Myers Squibb, Eisbach Bio, Immunocore, Novartis, Roche/Genentech, and Servier; his institution receives research funding from Bristol-Myers Squibb, Celgene, Eisbach Bio, and Roche/Genentech, and he holds ownership and serves on the Board of Directors of Pharma15, all outside the submitted work. Wolfgang Fendler reports fees from SOFIE Bioscience (research funding), Janssen (consultant, speakers' bureau), Calyx (consultant), Bayer (consultant, speakers' bureau, research funding), and Parexel (image review), as well as financial support from Mercator Research Center Ruhr (MERCUR, An-2019-0001), IFORES (D/107=81260, D/107=30240), and Wiedefeld-Stiftung/Stiftung Krebsforschung Duisburg, all outside the submitted work. No other potential conflict of interest relevant to this article was reported.

KEY POINTS

QUESTION: What is the ^{68}Ga -FAP PET uptake for different tumor entities?

PERTINENT FINDINGS: Mean SUV_{max} was significantly higher for ^{68}Ga -FAP than for ^{18}F -FDG in primary and metastatic pancreatic cancer lesions and in sarcoma. Mean TBR_{max} in primary lesions was better for ^{68}Ga -FAP than for ^{18}F -FDG in sarcoma, CCC, and cancers of the head and neck, prostate, pancreas, and pleura and was comparable for the remaining entities. Radiotracer uptake correlated positively with FAP expression levels in tissue samples. ^{68}Ga -FAP was superior to ^{18}F -FDG in detecting locoregional disease in sarcoma and distant metastatic disease in sarcoma, CCC, and cancers of the pancreas, head and neck, lung, and bladder.

IMPLICATIONS FOR PATIENT CARE: ^{68}Ga -FAP PET offers theranostic screening and has the potential for more precise staging and management of patients with these entities.

REFERENCES

- van Tinteren H, Hoekstra OS, Smit EF, et al. Effectiveness of positron emission tomography in the preoperative assessment of patients with suspected non-small-cell lung cancer: the PLUS multicentre randomised trial. *Lancet*. 2002;359:1388–1393.
- Ell PJ. The contribution of PET/CT to improved patient management. *Br J Radiol*. 2006;79:32–36.
- Choi JY, Lee KH, Shim YM, et al. Improved detection of individual nodal involvement in squamous cell carcinoma of the esophagus by FDG PET. *J Nucl Med*. 2000;41:808–815.
- Erdogan B, Ao M, White LM, et al. Cancer-associated fibroblasts promote directional cancer cell migration by aligning fibronectin. *J Cell Biol*. 2017;216:3799–3816.
- Gascard P, Tlsty TD. Carcinoma-associated fibroblasts: orchestrating the composition of malignancy. *Genes Dev*. 2016;30:1002–1019.
- Chen WT, Kelly T. Seprase complexes in cellular invasiveness. *Cancer Metastasis Rev*. 2003;22:259–269.
- Keane FM, Nadvi NA, Yao TW, Gorrell MD. Neuropeptide Y, B-type natriuretic peptide, substance P and peptide YY are novel substrates of fibroblast activation protein- α . *FEBS J*. 2011;278:1316–1332.
- Huang Y, Wang S, Kelly T. Seprase promotes rapid tumor growth and increased microvessel density in a mouse model of human breast cancer. *Cancer Res*. 2004;64:2712–2716.
- Kelly T. Fibroblast activation protein- α and dipeptidyl peptidase IV (CD26): cell-surface proteases that activate cell signaling and are potential targets for cancer therapy. *Drug Resist Updat*. 2005;8:51–58.
- Mueller SC, Ghersi G, Akiyama SK, et al. A novel protease-docking function of integrin at invadopodia. *J Biol Chem*. 1999;274:24947–24952.
- Lindner T, Loktev A, Altmann A, et al. Development of quinoline-based theranostic ligands for the targeting of fibroblast activation protein. *J Nucl Med*. 2018;59:1415–1422.
- Loktev A, Lindner T, Mier W, et al. A tumor-imaging method targeting cancer-associated fibroblasts. *J Nucl Med*. 2018;59:1423–1429.
- Giesel FL, Kratochwil C, Lindner T, et al. ^{68}Ga -FAP PET/CT: biodistribution and preliminary dosimetry estimate of 2 DOTA-containing FAP-targeting agents in patients with various cancers. *J Nucl Med*. 2019;60:386–392.
- Baum RP, Schuchardt C, Singh A, et al. Feasibility, biodistribution, and preliminary dosimetry in peptide-targeted radionuclide therapy of diverse adenocarcinomas using ^{177}Lu -FAP-2286: first-in-humans results. *J Nucl Med*. 2022;63:415–423.
- Ferdinandus J, Fragoso Costa P, Kessler L, et al. Initial clinical experience with ^{90}Y -FAP-46 radioligand therapy for advanced stage solid tumors: a case series of nine patients. *J Nucl Med*. 2022;63:727–734.
- Kratochwil C, Flechsig P, Lindner T, et al. ^{68}Ga -FAP PET/CT: tracer uptake in 28 different kinds of cancer. *J Nucl Med*. 2019;60:801–805.
- Kessler L, Ferdinandus J, Hirmas N, et al. ^{68}Ga -FAP as a diagnostic tool in sarcoma: data from the ^{68}Ga -FAP PET prospective observational trial. *J Nucl Med*. 2022;63:89–95.
- Ferdinandus J, Kessler L, Hirmas N, et al. Equivalent tumor detection for early and late FAP-46 PET acquisition. *Eur J Nucl Med Mol Imaging*. 2021;48:3221–3227.
- Kessler L, Ferdinandus J, Hirmas N, et al. Pitfalls and common findings in ^{68}Ga -FAP PET: a pictorial analysis. *J Nucl Med*. 2022;63:890–896.
- Harris PA, Taylor R, Minor BL, et al.; The REDCap consortium. Building an international community of software platform partners. *J Biomed Inform*. 2019;95:103208.
- Harris PA, Taylor R, Thielke R, Payne J, Gonzalez N, Conde JG. Research electronic data capture (REDCap): a metadata-driven methodology and workflow process for providing translational research informatics support. *J Biomed Inform*. 2009;42:377–381.
- Amin MB, Edge S, Greene F, et al. *AJCC Cancer Staging Manual*. 8th ed. Springer International Publishing; 2017:55–986.
- Lindner T, Loktev A, Giesel F, Kratochwil C, Altmann A, Haberkorn U. Targeting of activated fibroblasts for imaging and therapy. *EJNMMI Radiopharm Chem*. 2019;4:16.
- Loktev A, Lindner T, Burger EM, et al. Development of fibroblast activation protein-targeted radiotracers with improved tumor retention. *J Nucl Med*. 2019;60:1421–1429.
- Henry LR, Lee HO, Lee JS, et al. Clinical implications of fibroblast activation protein in patients with colon cancer. *Clin Cancer Res*. 2007;13:1736–1741.
- Hinkle DE, Wiersma W, Jurs SG. *Applied Statistics for the Behavioral Sciences*. 2nd ed. Houghton Mifflin; 2003:118.
- Lindner T, Altmann A, Kramer S, et al. Design and development of $^{99\text{m}}\text{Tc}$ -labeled FAP tracers for SPECT imaging and ^{188}Re therapy. *J Nucl Med*. 2020;61:1507–1513.
- Kratochwil C, Giesel FL, Rathke H, et al. [^{153}Sm]samarium-labeled FAP-46 radioligand therapy in a patient with lung metastases of a sarcoma. *Eur J Nucl Med Mol Imaging*. 2021;48:3011–3013.
- Kuyumcu S, Kovan B, Sanli Y, et al. Safety of fibroblast activation protein-targeted radionuclide therapy by a low-dose dosimetric approach using ^{177}Lu -FAP104. *Clin Nucl Med*. 2021;46:641–646.
- Assadi M, Rekabpour SJ, Jafari E, et al. Feasibility and therapeutic potential of ^{177}Lu -fibroblast activation protein inhibitor-46 for patients with relapsed or refractory cancers: a preliminary study. *Clin Nucl Med*. 2021;46:e523–e530.
- Narra K, Mullins SR, Lee HO, et al. Phase II trial of single agent Val-boroPro (Talabostat) inhibiting fibroblast activation protein in patients with metastatic colorectal cancer. *Cancer Biol Ther*. 2007;6:1691–1699.